BIOCHEMISTRY
including biophysical chemistry & molecular biology

Article

pubs.acs.org/biochemistry

p21 Exploits Residue Tyr151 as a Tether for High-Affinity PCNA Binding

Alice J. Kroker and John B. Bruning*

School of Biological Sciences, University of Adelaide, Adelaide, South Australia 5005, Australia

Supporting Information

ABSTRACT: Proliferating cell nuclear antigen (PCNA, processivity factor, sliding clamp) is a ring-shaped protein that tethers proteins to DNA in processes, including DNA replication, DNA repair, and cell-cycle control. Often used as a marker for cell proliferation, PCNA is overexpressed in cancer cells, making it an appealing pharmaceutical target. PCNA interacts with proteins through a PCNA interacting protein (PIP)-box, an eight-amino acid consensus sequence; different binding partners display a wide range of affinities based on function. Of all biological PIP-boxes, p21 has the highest known affinity for PCNA, allowing for inhibition of DNA replication and cell growth under cellular stress. As p21 is one of the few PIP-box sequences to contain a tyrosine rather than a phenylalanine in the eighth conserved position, we probed the significance of the hydroxyl group at this position using a mutational approach. Here we present the cocrystal structure of PCNA bound to a mutant p21 PIP-box peptide, p21Tyr151Phe, with associated isothermal titration calorimetry data. The p21Tyr151Phe peptide showed a 3-fold difference in affinity, as well as differences in entropy and enthalpy of binding. These differences can be attributed to a loss of hydrogen bonding capacity, as well as structural plasticity in the PCNA interdomain connector loop and the hydrophobic cavity of PCNA to which p21 binds. Thus, the hydroxyl group of Tyr151 in p21 acts as a tethering point for ideal packing and surface recognition of the peptide interface, increasing the binding affinity of p21 for PCNA.

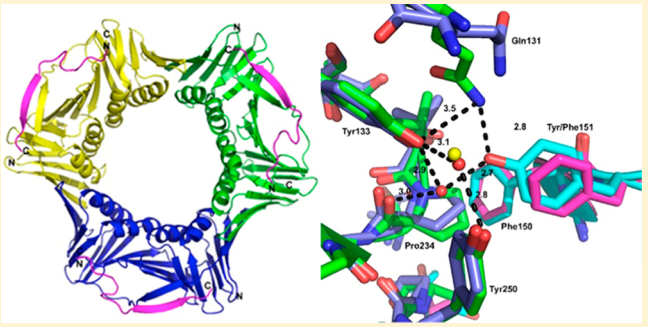

Proliferating cell nuclear antigen (PCNA), also known as the sliding clamp, is a nuclear protein with essential roles in DNA replication, DNA repair, and chromatin formation.[1] The function of PCNA is that of a molecular adaptor, tool belt, or docking platform, to control access to, recruitment to, and affinity of proteins for DNA and the replication fork.[2] PCNA is also a processivity factor, required for processive DNA polymerization by multiple polymerases, including the major replicative polymerase, Pol δ; PCNA increases the affinity of DNA Pol δ for DNA by 64000-fold.[3] In addition, PCNA interacts with a host of other partners, involved in processes such as Okazaki strand resolution, DNA repair, including mismatch repair, nucleotide excision repair, base excision repair, nonhomologous end joining, homologous recombination, and translesion synthesis, DNA modification, and cell-cycle control.[4]

Human PCNA is a ring-shaped, trimeric protein with pseudo 6-fold symmetry. Each subunit contains two similarly folded domains, each containing two α-helices and nine β-strands.[5,6] The α-helices line the center of the ring, while the β-strands form the outer surface of the ring. Within each subunit, the two domains are connected by the interdomain connector loop (IDCL) (residues 119−134), which runs along the outside of the ring.[6] The subunits are arranged in a head-to-tail manner, creating defined front and back faces.[7] The toroid structure allows for PCNA to encircle DNA and interact topologically to slide along it. This is facilitated by the positively charged inner surface, contributed by lysine and arginine residues within the α-helices, allowing for an electrostatic interaction between PCNA and the negatively charged backbone of DNA.[8,9] This overall structure is conserved in all sliding clamps across eukaryotes, prokaryotes, and archaea, despite a lack of sequence homology between different species.

Many of the proteins that interact with PCNA do so through a conserved motif coined the PCNA-interacting protein (PIP)-box.[10] The PIP-box is defined as Qxx[M/L/I]xx[F/Y][F/Y] and is usually, although not always, located in the C-terminal region of its interacting partners.[11] Almost 200 different biological PIP-boxes have been proposed from bioinformatics analysis.[12] Of the handful of PIP-boxes for which binding affinity data are available for the interaction with PCNA, differences in binding affinities have been reported.[3,13,14] Diversity in binding affinity is predicted to be a consequence of differences in the PIP-box consensus sequence and allow for the "tuning" of affinity relative to the role of the PCNA−PIP-box interaction, such that there is a link between binding affinity and protein function.

Of the biological PIP-boxes so far investigated, a key example is the p21 PIP-box. The levels of tumor suppressor protein p21

Received: March 6, 2015
Revised: May 13, 2015
Published: May 14, 2015

DOI: 10.1021/acs.biochem.5b00241
Biochemistry 2015, 54, 3483−3493

are elevated in response to DNA damage, not only to modulate cell-cycle progression by inhibiting cyclin-dependent kinases but also to interact directly with PCNA and block DNA replication and other processes, allowing DNA repair to occur prior to the resumption of replication.[6,10] This process is competitive, as p21 and Pol δ (p66 subunit) have both been shown through crystallographic studies to bind to the same site on PCNA.[3,6]

The p21 PIP-box has the highest known binding affinity for PCNA and is considered a model for high-affinity PCNA binding.[15] A p21 peptide containing the PIP-box has a 725-fold greater binding affinity for PCNA compared to that of an equivalent FEN1 peptide.[3] A structure of a p21 peptide containing the PIP-box (residues 139−160) has been crystallized in complex with human PCNA [Protein Data Bank (PDB) entry 1AXC].[6] This structure revealed that the PIP-box binding site is located near the IDCL of PCNA. The N-terminus of the peptide containing the PIP-box forms a 3_{10} helix that inserts into a hydrophobic pocket proximal to the IDCL on the surface of PCNA. The C-terminal end of the peptide forms an antiparallel β-sheet with the IDCL.[6] Several other PIP-box peptides have been crystallized in complex with human PCNA and also form the characteristic 3_{10} helix that inserts residues at positions 4, 7, and 8 of the PIP-box into the hydrophobic cavity of PCNA.[3,16,17] It has therefore been hypothesized that the residues at these three positions (4, 7, and 8) could be important for the interaction with PCNA and for tuning the degree of affinity. The PCNA−p21 crystal structure revealed that p21 Tyr151 (position 8 of the PIP-box) is involved in a water-mediated interaction with several PCNA residues.[6] The majority of PIP-boxes contain phenylalanine at this position, lacking the hydroxyl group observed in the p21 PIP-box (Table 1). This has led to the prediction that the Tyr151 residue in p21 could be, at least in part, responsible for the higher binding affinity of p21 for PCNA.

Table 1. Examples of Biological PIP-Box Sequences[a]

Protein	PIP-box
p21	QTSMTDFY
p66 (pol δ)	QVSITGFF
FEN1	QGRLDDFF
DNA pol η	MQTLESFF
DNA pol κ	KHTLDIFF
DNA pol ι	KKGLIDYY
RNase H2B	MKSIDTFF
MCMT	QTTITSHF
MSH3	QAVLSRFF
MSH6	QSTLYSFF
RecQ5	QNLIRHFF
UNG2	QKTLYSFF
WRN	QWKLLRDF
XPG	QLRIDSFF

[a]Conserved positions 1, 4, 7, and 8 that match the consensus sequence are highlighted.[3,6,8,11,16,17]

Misregulation of PCNA is associated with proliferative disorders such as cancer and is commonly used as a marker of cell proliferation.[18,19] PCNA levels have been reported to be 5−6-fold higher in cancer cells than in nonmalignant cells,[20] and the malignancy of several tumors has been directly correlated to PCNA expression levels.[21] Inhibition of PCNA, at the mRNA[21] and protein level,[10] has been shown to inhibit proliferation and cell growth, highlighting the protein as a potential anticancer target. Indeed, peptides and small molecule inhibitors of PCNA have been shown to be capable of selectively inhibiting malignant cell growth, in both cell culture and a mouse model.[15,22−28] Thyroid hormone T3 and its derivative, T2AA, have both been shown to bind to PCNA in the PIP-box binding site, thus inhibiting PIP-box binding. These small molecules were capable of inhibiting DNA replication and repair as well as sensitizing cells to the effects of the chemotherapeutic agent cisplatin.[15,22,26] However, no clinical trials have yet been undertaken with PCNA inhibitors, underscoring the need for a better understanding of the structural mechanism of its interacting partners. Current inhibitors often demonstrate low potency, cell permeability, bioavailability, and possible off-target effects. Peptide mimetics make up an approach to PCNA inhibition that has been suggested;[10] however, no such research has yet been performed.

In this study, we have used X-ray crystallography to determine the structure of PCNA in complex with a p21 peptide in which Tyr151 has been mutated to phenylalanine. This structure and the associated binding affinity calculated using isothermal titration calorimetry (ITC) have provided insight into the importance of residue 151 in the PCNA−p21 interaction. Binding affinity data revealed a 3-fold decrease in binding with the change of tyrosine to phenylalanine corresponding to a binding event that is enthalpically driven but has a reduced entropic term compared to that of wild-type binding. Our crystal structure not only shows the obvious loss of hydrogen bonding capacity compared to that of the wild-type structure but also demonstrates that shifts in the PCNA interdomain connector loop (IDCL) relative to the core structure and the hydrophobic cavity of PCNA to which p21 binds are key determinants of binding. Thus, the hydroxyl group of Tyr151 in p21 acts as a tethering point for ideal packing and surface recognition of the peptide interface, increasing the binding affinity of p21 for PCNA.

EXPERIMENTAL PROCEDURES

Computational Alanine Scanning. Computational alanine scanning was performed using a Robetta algorithm (http://robetta.bakerlab.org/alascansubmit.jsp).[29,30] PDB entry 1AXC was used as the input. $\Delta\Delta G$ was averaged across the three peptide−subunit complexes in the asymmetric unit.

Protein Expression. pET-28a-PCNA, which was cloned previously,[3] was transformed into BL21(DE3) cells. The bacterial culture was grown at 37 °C to an OD_{600} of 0.7 and induced using 0.5 mM IPTG at 16 °C for 16 h. Cells were harvested by centrifugation and cell pellets resuspended in 20 mM Tris (pH 8.0), 20 mM NaCl, 2 mM DTT, and 10% glycerol for ITC or 20 mM Tris (pH 7.5), 20 mM NaCl, 2 mM DTT, and 0.5 mM EDTA (pH 8.0) for crystallization. Resuspended cells were stored at −80 °C until they were purified.

PCNA Purification. Protein for ITC was produced as follows. Cells were lysed using high-pressure disruption

DOI: 10.1021/acs.biochem.5b00241
Biochemistry 2015, 54, 3483−3493

(Microfluidics cell disruptor), and the cell lysate was clarified by centrifugation. The clarified lysate was applied to a 5 mL DEAE Sepharose FF column (GE) and eluted with a linear NaCl gradient (0.1 to 0.5 M). Fractions containing PCNA were pooled and brought up to 1 M ammonium sulfate by the dropwise addition of 4 M ammonium sulfate, loaded onto a 5 mL HiTrap Phenyl FF column (GE), and eluted with a reverse linear gradient (1 to 0 M ammonium sulfate, 500 to 50 mM NaCl). Fractions containing PCNA were pooled and dialyzed overnight to 20 mM Tris (pH 7.5), 0.1 M NaCl, 10% glycerol, 2 mM DTT, and 0.5 mM EDTA. The sample was applied to an ENrich Q 5 × 50 column (Bio-Rad) and eluted with a linear NaCl gradient (0.2 to 0.8 M). Fractions containing PCNA were pooled and dialyzed overnight to 1× PBS for ITC.

Protein for crystallization was produced as follows. Cells were lysed using high-pressure disruption (Microfluidics cell disruptor), and the cell lysate was clarified by centrifugation. The clarified lysate was made up to 1.5 M ammonium sulfate by the dropwise addition of 4 M ammonium sulfate, applied to a HiTrap Phenyl FF column (GE), and eluted with a reverse linear gradient (1.5 to 0 M ammonium sulfate, 20 to 0 mM NaCl). Fractions containing PCNA were pooled and dialyzed to 20 mM Tris (pH 7.5), 20 mM NaCl, and 1 mM DTT. PCNA was applied to a HiTrap Q FF column (GE) and eluted with a linear NaCl gradient (20 to 700 mM). Fractions containing PCNA were pooled and dialyzed to 20 mM Tris (pH 7.5), 50 mM NaCl, and 1 mM DTT, then brought up to 1.5 M ammonium sulfate by the dropwise addition of 4 M ammonium sulfate, applied to a HiTrap Phenyl FF column (GE), and eluted with a reverse linear gradient (1.5 to 0 M ammonium sulfate, 20 to 0 mM NaCl). Fractions containing PCNA were pooled and dialyzed to 20 mM Tris (pH 7.5), 50 mM NaCl, and 1 mM DTT. PCNA was loaded onto a HiPrep 26/60 Sephacryl S-300 HR column (GE) equilibrated in 20 mM Tris (pH 7.5), 50 mM NaCl, and 1 mM DTT. Fractions containing PCNA were pooled and dialyzed to 20 mM Tris (pH 7.5), 10% glycerol, 0.5 mM EDTA, and 2 mM DTT. PCNA was concentrated to 12.6 mg/mL using an Amicon Ultra-15 Centrifugal Filter Unit (10 kDa molecular mass cutoff) and used fresh in crystallization experiments.

Peptide Synthesis. p21Tyr151Phe peptide (^{139}GRKRRQTSMTDFFHSKRRLIFS^{160}) was purchased from GenScript and synthesized at >95% purity by HPLC. Prior to being used in experiments, the lyophilized powder was resuspended in Tris (pH 8.0) and then dialyzed extensively to Tris (pH 7.5).

Isothermal Titration Calorimetry. Both peptide and PCNA solutions were dialyzed using either 500 or 10000 Da molecular mass cutoff dialysis tubing, respectively, to the same stock of PBS for 16 h at 4 °C prior to use in ITC experiments. Binding affinity data were determined using isothermal titration calorimetry (MicroCal iTC-200). PCNA was thermostated at 30 °C in the cell and the p21Tyr151Phe peptide injected stepwise over 20 injections. The initial PCNA concentration was 10 μM, and the initial peptide concentration was 270 μM. Data were fitted and analyzed using Origin 7 (MicroCal).

Crystallization. Cocrystals were produced using a 1:1 molar ratio (PCNA:peptide) at a final complex concentration of 0.44 mM. PCNA−p21Tyr151Phe cocrystals were grown by vapor diffusion in sitting drops at 16 °C; 1 μL of complex was mixed with 1 μL of well solution, containing 0.08 M strontium chloride hexahydrate, 0.02 M magnesium chloride hexahydrate, 0.04 M sodium cacodylate trihydrate (pH 7.0), 20% (v/v) (±)-2-methyl-2,4-pentanediol, and 0.012 M spermine tetrahydrochloride (Natrix G7, Hampton Research). The total volume of the well solution was 75 μL, and crystals were grown in a 96-well Intelliplate (Art Robbins). Hexagonal crystals grew to full size (approximately 250 μm in each dimension) within 1 week.

Data Collection and Processing. A single crystal was harvested without additional cryo-solution and cryo-cooled to 100 K for data collection. Diffraction data were collected at the Braggs Facility (University of Adelaide) using a Rigaku R-AXIS IV^{++} detector at a wavelength of 1.54 Å. Crystal diffraction data that extended to a resolution of 2.0 Å were collected using CrystalClear (Rigaku) and processed using iMosflm and Scala.[31,32] Data processing statistics are listed in Table 2.

Table 2. Crystallographic Data

Data Collection	
wavelength (Å)	1.54
space group	*P*3
unit cell dimensions	a = 142.97 Å, b = 142.97 Å, c = 41.41 Å, α = 90°, β = 90°, γ = 120°
resolution (Å)	41.4−2.0
no. of unique reflections	63391
average redundancy	7.1 (6.4)
completeness (%)	100 (99.9)
R_{merge}	0.051 (0.404)
I/σ	25.0 (3.8)
Refinement	
resolution (Å)	39.272−2.006
no. of protein atoms	7910
no. of water molecules	296
R_{free}	0.189
R_{work}	0.148
root-mean-square deviation	
bonds (Å)	0.002
angles (deg)	0.631
Ramachandran analysis	
no. of outliers	3 (0.3%)
no. favored	765 (95.7%)

Previous attempts to determine the structure involved hexagonal crystals grown in 0.1 M HEPES (pH 7.0) and 3.2 M ammonium sulfate (AmSO4 suite F10, Qiagen), cryo-protected with 20% glycerol, and cryo-cooled to 100 K for data collection. Diffraction data were recorded at the Australian Synchrotron on the MX1 beamline[33,34] to a resolution of 2.4 Å. The apparent space group was $P6_322$. Structures could not be determined because of the presence of twinning as has been reported previously for PCNA[3,6] and so was not pursued further.

Structure Refinement. The PCNA−p21Tyr151Phe crystal structure was determined by molecular replacement using Phaser MR.[35] The previously published PCNA−p21 structure (PDB entry 1AXC) was used as the search model, modified to contain a single PCNA subunit with a p21 peptide bound but missing the residue at position 151 to prevent bias. Three different PCNA subunit−p21Tyr151Phe peptide complexes were present within the asymmetric unit (ASU), with each subunit from a separate trimer. Three trimers were formed when the symmetry operators were applied to the monomers in the ASU, such that each trimer formed contained one subunit

DOI: 10.1021/acs.biochem.5b00241
Biochemistry 2015, 54, 3483−3493

from the ASU and two subunits that were symmetry mates (Figure 1 of the Supporting Information).

The presence of twinning in the crystal structure was identified using phenix.xtriage,[36] with the twin law $-h-kl$ and a near perfect twin fraction of 0.49. The true space group was *P*3, which generated an apparent space group of *P*6. Data, as well as twinning, were refined using phenix.refine and rebuilding performed in Coot.[37] Multiple rounds of refinement in Phenix followed by manual rebuilding in Coot were conducted until *R* factors converged. Molprobity and ADIT 2.0 were used for validation of the structure solution.[38,39] Crystal packing contacts are observed between some of the PCNA subunit−peptide complexes. As such, chains E and F were used for all structural analyses as no crystal contacts were found to interfere with the PCNA−peptide interaction. Likewise, the previous PCNA−p21 structure (PDB entry 1AXC) has several crystal packing contacts that possibly alter the PCNA−peptide interaction, so chains C and D were specifically chosen for comparison with our PCNA−peptide structure because of a lack of these contacts. Final refinement statistics are listed in Table 2.

Accession Number. Atomic coordinates and structure factors have been deposited in the PDB as entry 4RJF.

RESULTS

Energetic and Thermodynamic Analysis of the p21Tyr151Phe−PCNA Complex. While the p21 PIP-box remains the highest-affinity PIP-box for PCNA that has been measured experimentally, the amino acids that contribute most significantly to the p21 binding energy remain largely unexplored. A quantitative model of binding energies was implemented to delineate hot spots along the p21−PCNA interface that contribute most significantly to binding affinity. A computational model developed by Kortemme et al. was used, which is characterized by an all-atom rotamer description of interacting side chains combined with an energy function defined by hydrogen bonding, Lennard-Jones interactions, and solvation interactions;[29,30] this model was used to encompass the packing interactions and electrostatic interactions observed in the wild-type p21−PCNA cocrystal structure while using an implicit solvation model. The previously determined wild-type PCNA−p21 cocrystal structure was used to determine free energies of interaction, with successive alanine substitution at each position along the p21 peptide (PDB entry 1AXC). $\Delta\Delta G$ values ranged from 0.05 to 3.63 kcal mol^{-1} (see Table 3). The greatest $\Delta\Delta G$ determined within the PIP-box was for substitution of Tyr151 with alanine (3.55 kcal mol^{-1}), followed by Gln144, Met147, and Phe150 (3.06, 2.45, and 2.45 kcal mol^{-1}, respectively), which correspond to the conserved residues within the PIP-box. Because p21 is one of the few PIP-box peptides with a tyrosine in the second of the conserved aromatic positions of the PIP-box (rather than phenylalanine), the high value of the $\Delta\Delta G$ term suggests that the hydroxyl group of Tyr151 may be, at least in part, responsible for the high affinity of p21 compared to those of other PIP-box peptides (see Table 1 for a comparison of known PIP-box sequences and Figure 1 for an analysis of the frequency of amino acids at this position).

Given that computational approaches often ignore changes in backbone conformation or effects on the dynamics of interaction interfaces, the thermodynamic parameters and binding affinity of the peptide p21Tyr151Phe (residues 139−160) for PCNA were measured using ITC (the binding isotherm is shown in Figure 2). The Tyr151Phe mutation was engineered to probe the effect of the hydroxyl group of residue 151 on binding affinity, energetics of binding, and thermodynamic properties. This mutant p21-derived peptide was identical in length and composition to previously published p21−PCNA binding species (with the exception of the mutation of Tyr151 to phenylalanine),[3,6] allowing for straightforward comparison to the wild-type PCNA−p21 binding interaction. Fitting of the p21Tyr151Phe peptide binding data gave a stoichiometry of approximately 1:1, consistent with one peptide binding to one subunit or three peptides per trimer. The Gibbs free energy (ΔG), enthalpic (ΔH), and entropic ($T\Delta S$) terms are listed in Table 4. A 3-fold decrease in affinity was demonstrated for the p21Tyr151Phe peptide in comparison to that of the wild-type p21 peptide, corresponding to a shift in K_d from 83 nM for wild-type p21[3] to 250 nM for p21Tyr151Phe. The free energies of binding (ΔG) were similar for both peptides. Wild-type p21 showed binding (ΔH = −29.1 kcal mol^{-1}) 3-fold more enthalpically favorable than that of the Tyr151Phe mutant (−10.2 kcal mol^{-1}). Interestingly, the p21Tyr151Phe peptide showed a 15-fold difference in its entropy of binding compared to that of the wild-type peptide (a $T\Delta S$ value of 1.3 versus 19.3 kcal mol^{-1}). Consistent with previous PIP-box−PCNA interactions, the enthalpic terms are the favorable driving force in the Gibbs free energy equation. As such, the enthalpic term, which is not as favorable for the p21Tyr151Phe peptide, correlates with a decrease in binding affinity. Similarly, the FEN1 and p66 PIP-box peptides have a lower affinity in proportion to their lower enthalpic terms as compared to those of p21.[3] While the entropic term is unfavorable for the Tyr151Phe mutation, it is significantly more favorable than those of all previously reported PIP-box peptides, including the wild-type p21 PIP-box peptide.

Table 3. Energies of Binding Analysis by Amino Acid Residue for the p21−PCNA Complex (PDB entry 1AXC)[a]

residue no.	amino acid	$\Delta\Delta G$ (complex) (kcal mol^{-1})
144	Q	3.06
145	T	0.56
146	S	0.85
147	M	2.45
148	T	1.01
149	D	1.52
150	F	2.45
151	Y	3.55
152	H	0.10
153	S	0.40
154	K	0.05
155	R	1.76
156	R	3.63
157	L	0.34
158	I	1.96
159	F	0.26
160	S	0.98

[a] $\Delta\Delta G$ (complex) averaged across all three peptide−subunit complexes. See Experimental Procedures for experimental details.

Structure Solution and Global Fold of the p21Tyr151-Phe−PCNA Complex. The X-ray crystal structure of PCNA in complex with a mutant p21Tyr151Phe peptide (residues 139−160) was determined to a resolution of 2.0 Å by means of molecular replacement. The structure was determined in space

DOI: 10.1021/acs.biochem.5b00241
Biochemistry 2015, 54, 3483−3493

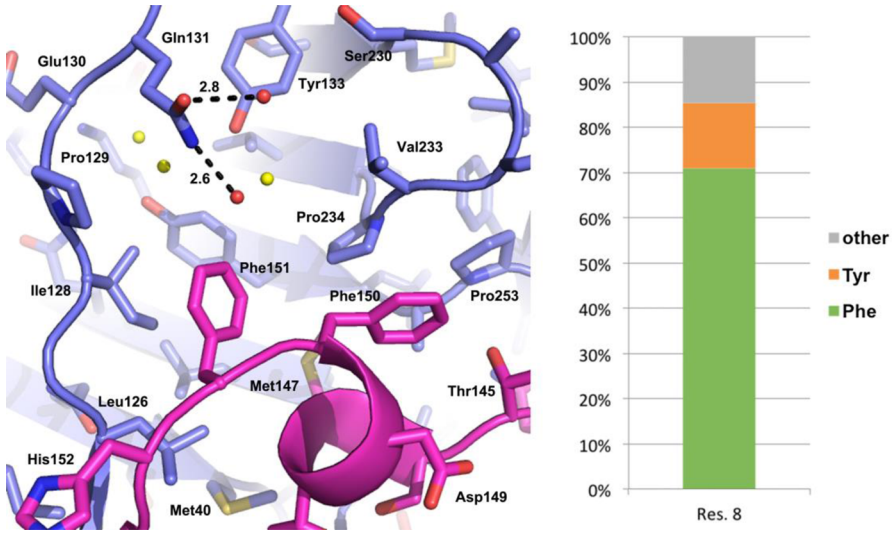

Figure 1. Position 8 of the PIP-box. Ribbon diagram of the p21Tyr151Phe (magenta) binding site on PCNA (blue) with side chains shown as sticks. Water molecules unique to the Tyr151Phe mutant structure are colored red, while others are colored yellow. To see water molecules involved in the bonding of hydrogen to PCNA, see Figure 5C. Chart illustrating the frequency of amino acid type at position 8 of the PIP-box (residue Tyr151 in p21) of all human PIP-boxes described in the literature as interacting with PCNA.[2−4,7,10,11,13,16,43−52]

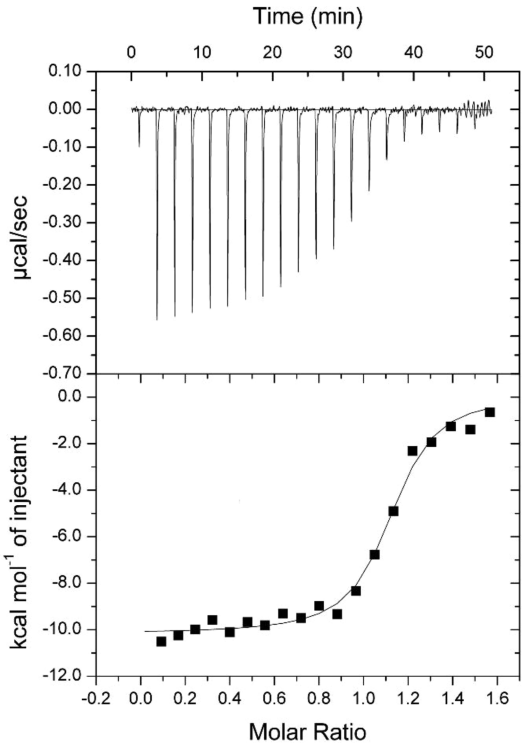

Figure 2. ITC measurements of the binding of the PIP-box-containing peptide p21Tyr151Phe (residues 139−160) to PCNA. Data were fit using a one peptide bound per subunit model. Thermodynamic parameters are listed in Table 4.

group *P*3 with an apparent space group *P*6 due to near perfect twinning (twin fraction of 0.49) with a twinning operator of $-h-kl$. PCNA crystallized with three subunits in the asymmetric unit, with one peptide bound per subunit. The three PCNA subunits were unambiguously modeled from residues 1−255, with poor electron density for the six C-terminal residues as well as two loops (residues 107−108 and 187−190) in two or one of the monomers, respectively; similar regions of disorder have been reported with previously

Table 4. PCNA Isothermal Titration Calorimetry with p21 and p21Tyr151Phe Peptides

	wild-type p21[3]	p21Tyr151Phe
N (stoichiometry)	1	1.1
K (affinity constant) (M^{-1})	1.21×10^7	4.00×10^6
ΔG (free energy) (kcal mol^{-1})	−9.8	−11.5
ΔH (enthalpy) (kcal mol^{-1})	−29.1	−10.2
ΔS (entropy) (cal mol^{-1} K^{-1})	−63.7	−4.4
$-T\Delta S$ (kcal mol^{-1})	19.3	1.3

determined PCNA crystal structures.[3,6,15−17,26] Of the peptide, 21, 20, or 18 residues were modeled unambiguously for each of chains B, D, and F, respectively. Ribbon diagrams of the PCNA subunit and trimer are shown in panels A and B of Figure 3, respectively. Reduced model bias difference Fourier maps of the p21Tyr151Phe peptide are shown in Figure 4. X-ray crystal structure processing and refinement statistics are listed in Table 1.

The PCNA structure (Figure 3A) has three subunits that are arranged in a head-to-tail fashion such that the N-terminal and C-terminal regions form subunit−subunit contacts, with the quaternary structure defined as a toroid, as shown in Figure 3B. The three subunits share a high degree of structural similarity with rmsd values between subunits ranging from 0.46 to 1.15 Å (over 253 Cα atoms) and surface area values ranging from 12611 to 12933 Å^2. Each subunit of PCNA contains 4 α-helices and 18 β-strands, with each of the domains in the subunit containing half of the α-helices and β-strands (two and nine, respectively). The PCNA trimer has pseudo 6-fold symmetry.

The p21Tyr151Phe peptide contacts the PCNA surface and shares an overall topology similar to those of previously reported PIP-box structures.[3,6,16,17] The three p21Tyr151Phe peptides share a high degree of structural homology, with rmsd values upon superimposition (over 18 Cα atoms) of 0.3 Å. The surface area of the three p21Tyr151Phe peptides ranges from 2600 to 2827 Å^2 with the area of the interface with PCNA ranging from 1076 to 1142 Å^2 (approximately 40% of the total surface area of the peptide). There are three distinct portions of the peptide: the N-terminal region (residues 139−145), a

DOI: 10.1021/acs.biochem.5b00241
Biochemistry 2015, 54, 3483−3493

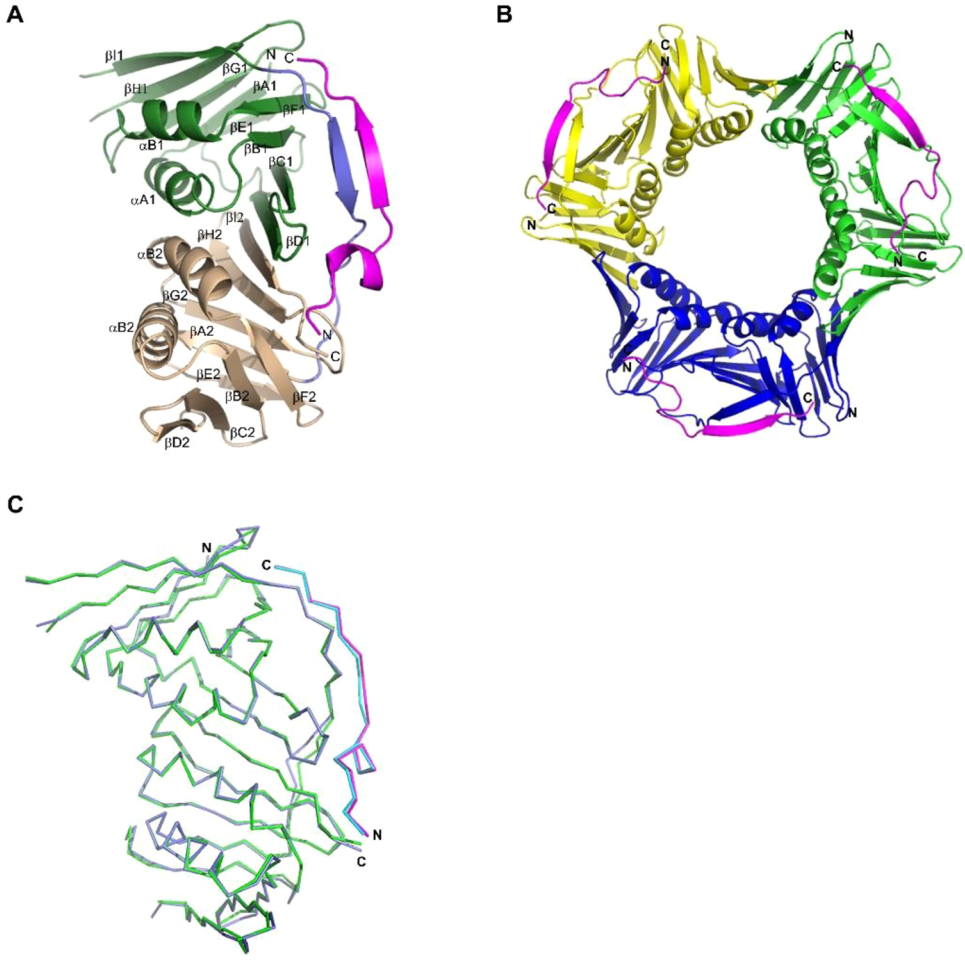

Figure 3. Global fold of the p21Tyr151Phe−PCNA cocrystal structure. (A) Ribbon diagram of the PCNA monomer. Domain 1 is colored green and domain 2 brown. The interdomain connector loop (IDCL) is colored blue. The p21 mutant peptide is colored magenta. (B) Ribbon diagram of the PCNA trimer. Individual subunits of PCNA are denoted by differences in color: yellow, green, and blue. Each p21Tyr151Phe peptide is colored magenta. (C) Wire diagram of the superimposition of the wild-type p21− and p21Tyr151Phe−PCNA cocrystal structures. PCNA is colored green for the wild-type structure (PDB entry 1AXC) and blue for the mutant-bound structure, while the wild-type p21 peptide is colored cyan and the mutant peptide magenta.

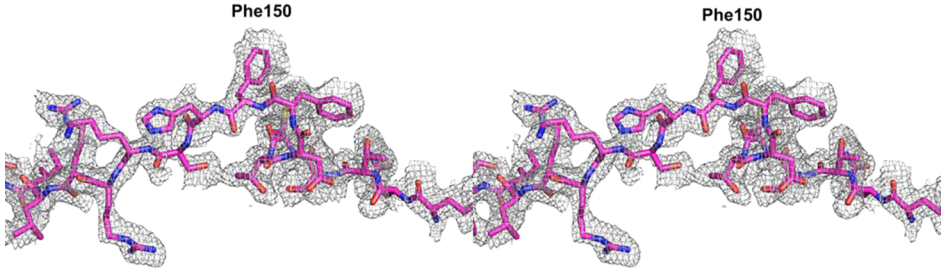

Figure 4. Electron density map of the p21Tyr151Phe peptide. The p21Tyr151Phe peptide is depicted as sticks in magenta with atoms colored by element. The electron density map is a $2F_o - F_c$ omit map contoured at 1σ. The diagram is in wall-eye stereo.

central portion that forms the characteristic 3_{10} helix (residues 146−151), and a C-terminal region (residues 152−160). The N-terminal region makes electrostatic interactions with the C-terminus of PCNA. The 3_{10} helix positions three residues (Ser146, Thr148, and Asp149) such that their side chains extend away from PCNA into the bulk solvent, while three other residues (Met147, Phe150, and Phe151) make contact in a hydrophobic pocket on the PCNA surface created between the IDCL and interdomain β-sheet of PCNA (Figures 5 and 6). The C-terminus of the peptide forms an antiparallel β-sheet with the IDCL of PCNA.

Comparison of Wild-Type p21− and p21Tyr151Phe−PCNA Cocrystal Structures. Both wild-type p21− and p21Tyr151Phe−PCNA cocrystal structures show a high degree of global similarity to the apo form of PCNA (PDB entry 1VYM)[40] upon superimposition, with an rmsd of 0.44 Å over 248 Cα atoms and 0.71 Å over 245 Cα atoms. From this, we deduce that no large-scale structural rearrangements of PCNA are required for or induced by peptide binding. Furthermore,

DOI: 10.1021/acs.biochem.5b00241
Biochemistry 2015, 54, 3483−3493

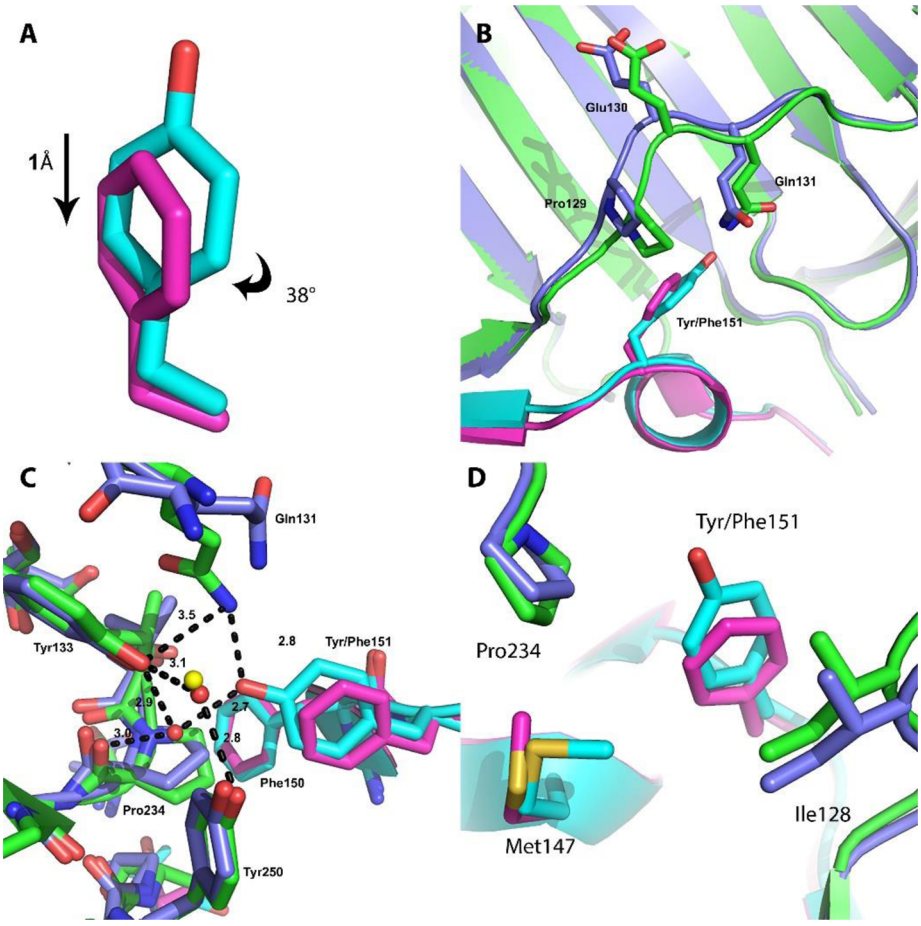

Figure 5. Comparison of the wild-type p21− and p21Tyr151Phe−PCNA cocrystal structures. Ribbon diagrams from a superimposition of PCNA (wild-type p21-bound PCNA and p21Tyr151Phe-bound PCNA), with interacting residues shown as sticks. PCNA bound to wild-type p21 is colored green, wild-type p21 cyan, PCNA bound to p21Tyr151Phe blue, and p21Tyr151Phe peptide magenta. (A) Comparison of the phenylalanine and tyrosine rotamers at position 151. (B) Comparison of the IDCL comprising the p21 binding pocket. (C) Comparison of the water-mediated hydrogen bond network proximal to Tyr151 of p21. Water molecules of the wild-type structure are colored red, while the water molecule in the p21Tyr151Phe-bound structure is colored yellow. For the sake of simplicity, only water molecules interacting with PCNA Tyr133, PCNA Tyr250, and p21 Tyr151 are shown here. (D) Comparison of the hydrophobic contacts at the Tyr151Phe binding site.

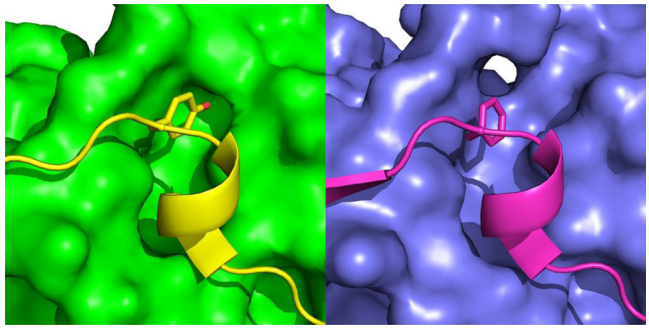

Figure 6. Surface representation of the p21−PCNA binding site. PCNA is depicted as a surface representation, while p21 is shown in ribbons with residue 151 shown as sticks. On the left is the wild-type p21−PCNA structure. PCNA is colored green and p21 yellow. On the right is the p21Tyr151Phe−PCNA structure. PCNA is colored blue and p21Tyr151Phe magenta.

the wild-type p21- and p21Tyr151Phe-bound PCNA structures share a high degree of structural similarity upon being superimposed with an rmsd of 0.43 Å over 248 Cα atoms, implying that differences in affinity and thermodynamic parameters are subtle and localized to the p21−PCNA interface. The superimposition of wild-type and mutant structures is shown in Figure 3C. Superimposition of only the p21 wild-type and Tyr151Phe peptide chains reveals an rmsd value of 0.37 Å over 18 Cα atoms highlighting that both peptides adopt nearly identical topology when bound to PCNA. Calculation of the interface area for the PIP-box region of both peptides (residues 143−152) shows that the p21Tyr151Phe interface area is slightly smaller with a value of 564.4 Å^2 versus 607.3 Å^2 for wild-type p21-bound PCNA, consistent with an extra hydroxyl group for interaction in the wild-type structure and expansion of the cavity size in the mutant structure. Interestingly, the hydrophobic cavity into which residue 151 docks was larger for the mutant structure: 223.6 Å^3 for the p21Tyr151Phe structure compared to 98.9 Å^3 for the wild-type structure, a nearly 2.3-fold expansion in pocket volume (calculated using CASTp[41]). Differences in cavity volume are presented in Figure 6.

Tyr151 of the wild-type p21 peptide participates in not only direct electrostatic interactions but also water-mediated hydrogen bonds, as well as hydrophobic and van der Waals interactions. Wild-type p21 Tyr151 forms a hydrogen bond with Gln131 of the PCNA IDCL (2.8 Å from a lone pair of carbonyl oxygen of the Tyr151 side chain to Nϵ of the Gln131

DOI: 10.1021/acs.biochem.5b00241
Biochemistry 2015, 54, 3483−3493

side chain) as seen in Figure 5C. In addition to the formation of a hydrogen bond with Tyr151, Gln131 is also found within weak hydrogen bonding distance of Tyr133 of PCNA (3.5 Å from Nε of the Gln151 side chain to the Tyr133 carbonyl oxygen of the side chain). Two water molecules are found in the wild-type p21 structure proximal to Tyr151, both involved in a web of interactions stabilizing the PCNA binding surface. The oxygen atom of the Tyr151 side chain is 2.7 Å from a water molecule, which in turn forms two other hydrogen bonds: 3 Å to the backbone carbonyl of Pro234 and 2.9 Å to the oxygen atom of the Tyr133 side chain, both of PCNA. The second water molecule is not bonded to p21 Tyr151 but rather forms a water-mediated hydrogen bond between the side chain oxygen atoms of PCNA residues Tyr133 (3.1 Å) and Tyr250 (2.8 Å), aiding in the stability of the p21 binding surface. The hydrophobic and van der Waals contacts through Tyr151 of wild-type p21 are responsible for much of the packing of the 3_{10} helix "hydrophobic plug" into the cavity on the PCNA surface, known as the "hydrophobic pocket". These contacts include the side chains of PCNA residues Pro234 and Ile128 as well as Met147 of p21 (Figure 5D).

Mutation of Tyr151 to phenylalanine in the p21 peptide means a loss of both hydrogen bond donor and acceptors on the side chain and results in structural rearrangements in the IDCL, changes in the hydrophobic packing of the 3_{10} helix, and disruption of part of the extensive hydrogen bonding network at the PCNA−p21 interface. The PCNA−p21Tyr151Phe cocrystal structure shows that Phe151, in comparison to Tyr151, is not positioned similarly or as closely to the PCNA surface, with the phenyl ring 1 Å farther from the PCNA surface and the rotamer rotated 38° (Figure 5A). The inability to hydrogen bond results in several structural alterations. PCNA Gln131 no longer forms a hydrogen bond with Phe151, allowing for a shift in the Gln131 side chain of approximately 2 Å away from PCNA and toward the bulk solvent (Figure 5C). This shift in Gln131 position precludes hydrogen bonding to PCNA Tyr133 as occurs in the wild-type structure. As a result, the portion of the IDCL comprising residues 127−131 is not as well tethered to the binding surface of PCNA as in the wild-type structure and is found to be shifted approximately 2 Å from PCNA toward the bulk solvent (Figure 5B). No water-mediated hydrogen bond can be formed between p21 Phe151 and PCNA; however, the PCNA residues Tyr133 and Pro234 that are involved in water-mediated hydrogen bonds with Tyr151 in the wild-type structure are unaffected by the mutation to Phe151 and are found in positions nearly identical to those in the wild-type p21−PCNA cocrystal (Figure 5C). The ability of PCNA residues such as Tyr133 and Tyr250 to maintain the proper conformation for p21 binding is bolstered by the fact that the water-mediated hydrogen bond between the two is also found in the mutant structure; mutation to phenylalanine at position 151 of p21 has no effect on water-mediated hydrogen bonds to residues Tyr133 and Tyr250. The shift in the phenyl ring of Phe151 in the mutant structure away from the PCNA binding surface affects the hydrophobic packing of the 3_{10} helix into the hydrophobic pocket (Figure 5D). The side chains of PCNA residues Pro234 and Ile128 as well as p21 Met147 are not as close to the phenyl ring of p21 Phe151, shifted approximately 1 Å outward from the cavity. This expansion of the cavity results in looser packing and a weaker overall hydrophobic affinity of the p21 peptide for PCNA within the hydrophobic pocket. Interestingly, the lack of an oxygen atom at the terminus of the Phe151 side chain (as is in the wild-type structure), combined with an overall expansion of the pocket, has allowed for the identification of three water molecules not previously reported (Figure 1, left panel). Two are found within hydrogen bonding distance of PCNA Gln131 (2.6 and 2.8 Å), and the last is located in the proximity of where the oxygen atom of the side chain of p21 Tyr151 lies in the wild-type structure (1.6 Å from the oxygen atom of Tyr151 upon superimposition of the structures). None of these water molecules hydrogen bond with p21.

DISCUSSION

While PCNA interacting partners interact with PCNA via the PIP-box consensus sequence, they can display wide variations in binding affinity. For example, the FEN1 PIP-box affinity for PCNA is 725-fold weaker than that of the p21 PIP-box. What is the structural basis for this large difference in affinity among PIP-box peptides? What interactions are critical for optimizing high affinity? These questions have been difficult to answer to date because comparisons have been drawn between only very dissimilar sequences. PIP-box sequences used in structural studies thus far have been too convoluted to dissect the residue by residue impacts on affinity. The limited structural information about the PCNA−PIP-box interaction mechanism is hampering our ability to interpret and explain the hierarchy of binding affinities that exists. To overcome this, we have here chosen a mutational approach that has allowed us to directly probe the significance of Tyr151, a p21 residue previously hypothesized to be critical for high affinity, by means of structure, affinity, and energetic considerations compared to the wild-type p21 sequence. We can now directly measure the significance of Tyr151 in p21 affinity for PCNA and begin to answer the question of which binding epitopes are critical for high-affinity binding to PCNA.

Comparison of the thermodynamic properties of binding revealed differences in binding energetics between the p21 wild-type and Tyr151Phe peptides. All PIP-box peptides measured thus far have shown that negative enthalpic terms are the driving force for the negative Gibbs free energy of binding, including for the p21 wild-type and Tyr151Phe peptides. Comparison of the two enthalpic terms shows that the wild-type peptide (-29 kcal mol^{-1}) is nearly 3 times more favorable in enthalpy (-10 kcal mol^{-1}). Because both peptides have nearly identical overall Gibbs free energies of binding, the decrease in enthalpic favorability is offset in the mutant peptide by a decrease in the value of the entropy term; the p21Tyr151Phe peptide bears a much lower entropic penalty upon binding (-4.4 cal mol^{-1} K^{-1} for the mutant vs -63.7 cal mol^{-1} K^{-1} for the wild type). Because previous studies have shown a loose trend that correlates binding affinity of PIP-boxes with the negativity of Gibbs free energy, it is not surprising that the binding affinity of the mutant, while decreased, is not majorly reduced (K_d of 250 nM vs K_d of 82.6 nM) as the Gibbs free energies of binding are quite similar for both. However, tyrosine instead of phenylalanine at this position imparts an advantage in binding affinity, albeit only a modest advantage (approximately 3-fold).

The hydroxyl group of p21 Tyr151 forms a structural tethering point to PCNA, which can explain an effect on not only affinity but also the packing of the 3_{10} helix, entropic considerations in binding, and effects on enthalpy. The hydroxyl group of Tyr151 forms a tether to PCNA through hydrogen bonding to Gln131 (2.8 Å) as well as water-mediated (2.7 Å to the water molecule) hydrogen bonding to Tyr133 and

DOI: 10.1021/acs.biochem.5b00241
Biochemistry 2015, 54, 3483−3493

Pro234 (Figure 5C). The immediate effect of this tether is that the aromatic ring is pulled deeper into the binding cavity of PCNA; this depth is >1 Å as measured by comparison of the p21 mutant and wild-type structures (Figure 5A). The lack of a hydrogen bonding network in the p21Tyr151Phe structure is the most likely explanation for the decrease in the favorable enthalpy of binding as compared to the wild-type binding mode. The Tyr151 tether has the effect of creating tighter packing as seen by comparison to the mutant structure in which the IDCL (residues 127−131) is packing nearly 2 Å farther away, as well as the hydrophobic contacts, including PCNA residues Ile128 and Pro234 and p21 residue Met147, which are nearly 1 Å farther away (Figures 5D and 6). This is also highlighted by the 43 Å^2 difference in interaction surface area between the mutant and wild type. We hypothesize that these structural rearrangements required to facilitate the tighter packing in the wild-type structure are the reason for the higher entropic penalty of binding as compared to that of the p21Tyr151Phe structure. Interestingly, water-mediated hydrogen bonding that is independent of p21 Tyr151 is retained in the p21Tyr151Phe structure between PCNA residues Tyr250 and Tyr133, with these residues found in identical positions in both structures. This infers that this portion of the binding pocket is not affected by hydrogen bonding to p21 and that the water molecule helps form the binding pocket independently and potentially prior to binding.

While it is obvious that removal of the hydroxyl group from Tyr151 of p21 would likely affect the binding affinity and the enthalpic contribution to binding, it is surprising that the reduction in affinity is only 3-fold when other PIP-box sequences bearing a phenylalanine at this position have markedly reduced binding affinities compared to those of p21, reduced by several hundred-fold. The structural rearrangements of both the IDCL and residues of the hydrophobic pocket were not predicted and suggest that high-affinity binding relies, in part, on an entropic penalty of binding that can be overcome by the overall enthalpic nature of the binding mechanism. The significance of this mutation from tyrosine to phenylalanine and the observations made is that at the eighth position of the PIP-box the majority of biological PIP-boxes identified have phenylalanine (which lacks the ability to be tethered) rather than tyrosine (capable of being tethered) (Figure 1, right panel). Of the handful of biological PIP-boxes that do have tyrosine, p21 is the only PIP-box for which there are binding affinity data currently available, so this study is the first time that the significance of tyrosine at this position of the PIP-box has truly been shown. Identifying the determinants of high-affinity PCNA binding lends itself to a mutagenesis approach, so that the significance of differences in the PIP-box can be determined residue by residue. As a tyrosine residue at position 8 of the PIP-box is relatively unique to p21, it is anticipated that differences in the frequency of residues at other conserved sites of the consensus PIP-box will provide hints about critical residues that contribute to high-affinity binding. The determinants of the high affinity of p21 over other PCNA-interacting proteins are likely to be multiple and will require more experiments to decipher completely.

The affinity and structure of a small number of PIP-box peptides that contain Phe in the second conserved aromatic position have been previously studied. These include the p66 PIP-box (K_d = 15.6 μM), the FEN1 PIP-box (K_d = 60 μM), and the nonphysiological PIP-box, the PL peptide (K_d = 100 nM).[3,40] These results, coupled with our mutational results, demonstrate that affinity can largely be modulated by alteration of residues outside of the second conserved aromatic position. The structural mechanism of the differential affinity of these Phe-containing PIP-boxes has been difficult to determine because of the degeneracy of the PIP-box sequence, especially the residues of the 3_{10} helix. The structures containing Phe in the second aromatic residue of the PIP-box bound to human PCNA can be seen in Figure 7. Superimposition of the mutant

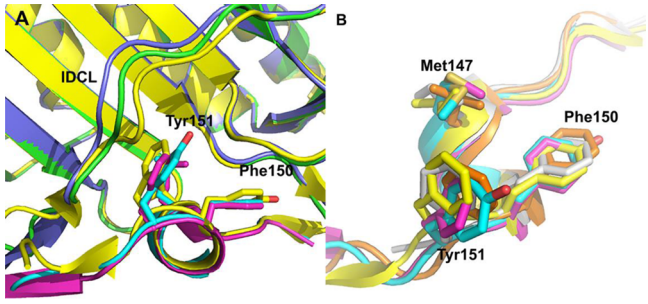

Figure 7. Comparison of PIP-box peptides bound to human PCNA that contain Phe at PIP-box conserved residue 8. Crystal structures were superimposed, and colors represent the following: yellow, PL peptide−PCNA complex (PDB entry 1VYJ); blue, PCNA from the Tyr151Phe complex (PDB entry 4RJF); magenta, p21Tyr151Phe peptide from the Tyr151Phe complex (PDB entry 4RJF); green, PCNA from the wild-type p21 complex (PDB entry 1AXC); cyan, p21 peptide in the wild-type p21−PCNA complex (PDB entry 1AXC); orange, FEN1−PCNA complex (PDB entry 1U7B); and gray, p66−PCNA complex (PDB entry 1U76). (A) Superimposition of PCNA in complex with the p21 wild-type peptide, the Tyr151Phe peptide, and the PL peptide to demonstrate the effect on the IDCL. (B) Superimposition of the 3_{10} helix of PIP-box peptides FEN1, p66, p21, PL peptide, and p21Tyr151Phe.

p21Y151F structure with the PL PIP-box peptide and wild-type p21 peptide structures reveals that the IDCL in the PL peptide structure is drawn closer to the 3_{10} helix by approximately 1.6 Å (as compared to that of wild-type p21), which is in contrast to the p21Tyr151Phe peptide structure, where the IDCL is shifted nearly 2 Å from the 3_{10} helix toward the bulk solvent (Figure 7A). The PL peptide contains a Tyr rather than a Phe in the first conserved aromatic residue of the PIP-box, contains an Ile rather than a Met in the fourth conserved position of the PIP-box, and has several different residues in the variable regions of the PIP-box as compared to p21; these differences may account for the differential packing of the IDCL and the residues of the hydrophobic pocket in the PL structure. Superimposition of the peptides containing Phe at the second conserved aromatic residue of the PIP-box (Figure 7B) shows that the side chains and position of the 3_{10} helix backbone atoms adopt quite variable conformations; however, the conformations of these side chains are most similar to those of the Tyr151Phe mutant structure (Figure 5). From this, we conclude that our mutational approach has allowed us to most accurately (in contrast to comparison to the FEN1, p66, and PL peptide structures) deduce the effect of the Tyr151 residue on affinity and structure. Furthermore, residues other than Tyr151 that pack in the hydrophobic pocket of PCNA such as p21 residues Met147 and Phe150, as well as residues in the variable positions of the PIP-box (positions 2, 3, 5, and 6), likely make strong contributions to PIP-box affinity for PCNA through packing interactions and positioning of the 3_{10} helix.

DOI: 10.1021/acs.biochem.5b00241
Biochemistry 2015, 54, 3483−3493

PCNA−PIP-box interactions may not have been fully optimized during evolution to be high-affinity[42] to ensure the ability of the "tools" to be changed on the "belt" while still maintaining the hierarchy of binding. Our results have revealed that the tyrosine at the last position of the PIP-box makes a contribution to the high affinity of p21 for PCNA. As such, a small molecule or peptide mimetic inhibitor would aim to include or even further encourage this interaction, such as by providing a hydroxyl group for involvement in the interaction, or even extending the residue side chain to replace the water molecule, such that the interaction is then direct rather than water-mediated.

■ ASSOCIATED CONTENT

Supporting Information

Supplemental Figures 1 and 2. The Supporting Information is available free of charge on the ACS Publications website at DOI: 10.1021/acs.biochem.5b00241.

■ AUTHOR INFORMATION

Corresponding Author

*School of Biological Sciences, University of Adelaide, Adelaide, South Australia, Australia. E-mail: john.bruning@adelaide.edu.au. Telephone: +61 (08) 8313-5218. Fax: +61 (08) 8313-4362.

Author Contributions

A.J.K. performed protein purification, ITC, protein cocrystallization, and structure solution and helped with manuscript preparation. J.B.B. managed and contributed to structure solution, data collection, and manuscript preparation.

Funding

Synchrotron funding was provided by Australian Synchrotron Grant AS133/MXCAP/6919.

Notes

The authors declare no competing financial interest.

■ ACKNOWLEDGMENTS

We acknowledge the support of the Bragg's Facility for our home source data collection and the Australian Synchrotron for help with data collection and detwinning. This research was undertaken on the MX1 beamline at the Australian Synchrotron, Victoria, Australia.

■ ABBREVIATIONS

ASU, asymmetric unit; DEAE, diethylaminoethyl; DTT, dithiothreitol; EDTA, ethylenediaminetetraacetic acid; FEN1, flap endonuclease 1; HPLC, high-pressure liquid chromatography; IDCL, interdomain connector loop; ITC, isothermal titration calorimetry; mRNA, messenger ribonucleic acid; PCNA, proliferating cell nuclear antigen; PIP-box, PCNA-interacting protein-box; rmsd, root-mean-square deviation.

■ REFERENCES

(1) Moldovan, G. L., Pfander, B., and Jentsch, S. (2007) PCNA, the maestro of the replication fork. *Cell 129* (4), 665−679.

(2) Mailand, N., Gibbs-Seymour, I., and Bekker-Jensen, S. (2013) Regulation of PCNA-protein interactions for genome stability. *Nat. Rev. Mol. Cell Biol. 14* (5), 269−282.

(3) Bruning, J. B., and Shamoo, Y. (2004) Structural and thermodynamic analysis of human PCNA with peptides derived from DNA polymerase-δ p66 subunit and flap endonuclease-1. *Structure 12* (12), 2209−2219.

(4) De Biasio, A., and Blanco, F. J. (2013) Proliferating cell nuclear antigen structure and interactions: Too many partners for one dancer? *Adv. Protein Chem. Struct. Biol. 91*, 1−36.

(5) Krishna, T. S., Kong, X. P., Gary, S., Burgers, P. M., and Kuriyan, J. (1994) Crystal structure of the eukaryotic DNA polymerase processivity factor PCNA. *Cell 79* (7), 1233−1243.

(6) Gulbis, J. M., Kelman, Z., Hurwitz, J., O'Donnell, M., and Kuriyan, J. (1996) Structure of the C-terminal region of p21(WAF1/CIP1) complexed with human PCNA. *Cell 87* (2), 297−306.

(7) Maga, G., and Hubscher, U. (2003) Proliferating cell nuclear antigen (PCNA): A dancer with many partners. *J. Cell Sci. 116* (Part 15), 3051−3060.

(8) Dieckman, L. M., Freudenthal, B. D., and Washington, M. T. (2012) PCNA Structure and Function: Insights from Structures of PCNA Complexes and Post-translationally Modified PCNA. *Subcell. Biochem. 62*, 281−299.

(9) Georgescu, R. E., Kim, S. S., Yurieva, O., Kuriyan, J., Kong, X. P., and O'Donnell, M. (2008) Structure of a sliding clamp on DNA. *Cell 132* (1), 43−54.

(10) Warbrick, E., Lane, D. P., Glover, D. M., and Cox, L. S. (1995) A small peptide inhibitor of DNA replication defines the site of interaction between the cyclin-dependent kinase inhibitor p21WAF1 and proliferating cell nuclear antigen. *Curr. Biol. 5* (3), 275−282.

(11) Warbrick, E. (1998) PCNA binding through a conserved motif. *BioEssays 20* (3), 195−199.

(12) Gilljam, K. M., Feyzi, E., Aas, P. A., Sousa, M. M., Muller, R., Vagbo, C. B., Catterall, T. C., Liabakk, N. B., Slupphaug, G., Drablos, F., Krokan, H. E., and Otterlei, M. (2009) Identification of a novel, widespread, and functionally important PCNA-binding motif. *J. Cell Biol. 186* (5), 645−654.

(13) De Biasio, A., Campos-Olivas, R., Sanchez, R., Lopez-Alonso, J. P., Pantoja-Uceda, D., Merino, N., Villate, M., Martin-Garcia, J. M., Castillo, F., Luque, I., and Blanco, F. J. (2012) Proliferating cell nuclear antigen (PCNA) interactions in solution studied by NMR. *PLoS One 7* (11), e48390.

(14) Zheleva, D. I., Zhelev, N. Z., Fischer, P. M., Duff, S. V., Warbrick, E., Blake, D. G., and Lane, D. P. (2000) A quantitative study of the in vitro binding of the C-terminal domain of p21 to PCNA: Affinity, stoichiometry, and thermodynamics. *Biochemistry 39* (25), 7388−7397.

(15) Punchihewa, C., Inoue, A., Hishiki, A., Fujikawa, Y., Connelly, M., Evison, B., Shao, Y., Heath, R., Kuraoka, I., Rodrigues, P., Hashimoto, H., Kawanishi, M., Sato, M., Yagi, T., and Fujii, N. (2012) Identification of small molecule proliferating cell nuclear antigen (PCNA) inhibitor that disrupts interactions with PIP-box proteins and inhibits DNA replication. *J. Biol. Chem. 287* (17), 14289−14300.

(16) Hishiki, A., Hashimoto, H., Hanafusa, T., Kamei, K., Ohashi, E., Shimizu, T., Ohmori, H., and Sato, M. (2009) Structural basis for novel interactions between human translesion synthesis polymerases and proliferating cell nuclear antigen. *J. Biol. Chem. 284* (16), 10552−10560.

(17) Bubeck, D., Reijns, M. A., Graham, S. C., Astell, K. R., Jones, E. Y., and Jackson, A. P. (2011) PCNA directs type 2 RNase H activity on DNA replication and repair substrates. *Nucleic Acids Res. 39* (9), 3652−3666.

(18) Miyachi, K., Fritzler, M. J., and Tan, E. M. (1978) Autoantibody to a nuclear antigen in proliferating cells. *J. Immunol. 121* (6), 2228−2234.

(19) Bravo, R., Fey, S. J., Bellatin, J., Larsen, P. M., Arevalo, J., and Celis, J. E. (1981) Identification of a nuclear and of a cytoplasmic polypeptide whose relative proportions are sensitive to changes in the rate of cell proliferation. *Exp. Cell Res. 136* (2), 311−319.

(20) Naryzhny, S. N., and Lee, H. (2007) Characterization of proliferating cell nuclear antigen (PCNA) isoforms in normal and cancer cells: There is no cancer-associated form of PCNA. *FEBS Lett. 581* (25), 4917−4920.

(21) Sakakura, C., Hagiwara, A., Tsujimoto, H., Ozaki, K., Sakakibara, T., Oyama, T., Ogaki, M., and Takahashi, T. (1994) Inhibition of gastric cancer cell proliferation by antisense oligonucleotides targeting

DOI: 10.1021/acs.biochem.5b00241
Biochemistry 2015, 54, 3483−3493

the messenger RNA encoding proliferating cell nuclear antigen. *Br. J. Cancer 70* (6), 1060−1066.
(22) Actis, M., Inoue, A., Evison, B., Perry, S., Punchihewa, C., and Fujii, N. (2013) Small molecule inhibitors of PCNA/PIP-box interaction suppress translesion DNA synthesis. *Bioorg. Med. Chem. 21*, 1972−1977.
(23) Cayrol, C., Knibiehler, M., and Ducommun, B. (1998) p21 binding to PCNA causes G1 and G2 cell cycle arrest in p53-deficient cells. *Oncogene 16* (3), 311−320.
(24) Dillehay, K. L., Lu, S., and Dong, Z. (2014) Anti-tumor effects of a novel small molecule targeting PCNA chromatin association in prostate cancer. *Mol. Cancer Ther.*, 2817−2826.
(25) Gu, L., Smith, S., Li, C., Hickey, R. J., Stark, J. M., Fields, G. B., Lang, W. H., Sandoval, J. A., and Malkas, L. H. (2014) A PCNA-Derived Cell Permeable Peptide Selectively Inhibits Neuroblastoma Cell Growth. *PLoS One 9* (4), e94773.
(26) Inoue, A., Kikuchi, S., Hishiki, A., Shao, Y., Heath, R., Evison, B. J., Actis, M., Canman, C. E., Hashimoto, H., and Fujii, N. (2014) A Small Molecule Inhibitor of Monoubiquitinated Proliferating Cell Nuclear Antigen (PCNA) Inhibits Repair of Interstrand DNA Cross-link, Enhances DNA Double Strand Break, and Sensitizes Cancer Cells to Cisplatin. *J. Biol. Chem. 289* (10), 7109−7120.
(27) Massodi, I., Bidwell, G. L., III, and Raucher, D. (2005) Evaluation of cell penetrating peptides fused to elastin-like polypeptide for drug delivery. *J. Controlled Release 108* (2−3), 396−408.
(28) Tan, Z., Wortman, M., Dillehay, K. L., Seibel, W. L., Evelyn, C. R., Smith, S. J., Malkas, L. H., Zheng, Y., Lu, S., and Dong, Z. (2012) Small-molecule targeting of proliferating cell nuclear antigen chromatin association inhibits tumor cell growth. *Mol. Pharmacol. 81* (6), 811−819.
(29) Kortemme, T., and Baker, D. (2002) A simple physical model for binding energy hot spots in protein-protein complexes. *Proc. Natl. Acad. Sci. U.S.A. 99* (22), 14116−14121.
(30) Kortemme, T., Kim, D. E., and Baker, D. (2004) Computational alanine scanning of protein-protein interfaces. *Sci. STKE 2004* (219), 1−8.
(31) Leslie, A. G., and Powell, H. R. (2007) Processing Diffraction Data with Mosflm. In *Evolving Methods for Macromolecular Crystallography*, Vol. *245*, pp 41−51, Springer, Berlin.
(32) Winn, M. D., Ballard, C. C., Cowtan, K. D., Dodson, E. J., Emsley, P., Evans, P. R., Keegan, R. M., Krissinel, E. B., Leslie, A. G., McCoy, A., McNicholas, S. J., Murshudov, G. N., Pannu, N. S., Potterton, E. A., Powell, H. R., Read, R. J., Vagin, A., and Wilson, K. S. (2011) Overview of the CCP4 suite and current developments. *Acta Crystallogr. D67* (Part 4), 235−242.
(33) Cowieson, N. P., Aragao, D., Clift, M., Ericsson, D. J., Gee, C., Harrop, S. J., Mudie, N., Panjikar, S., Price, J. R., Riboldi-Tunnicliffe, A., Williamson, R., and Caradoc-Davies, T. (2015) MX1: A bending-magnet crystallography beamline serving both chemical and macromolecular crystallography communities at the Australian Synchrotron. *J. Synchrotron Radiat. 22* (Part 1), 187−190.
(34) McPhillips, T. M., McPhillips, S. E., Chiu, H. J., Cohen, A. E., Deacon, A. M., Ellis, P. J., Garman, E., Gonzalez, A., Sauter, N. K., Phizackerley, R. P., Soltis, S. M., and Kuhn, P. (2002) Blu-Ice and the Distributed Control System: Software for data acquisition and instrument control at macromolecular crystallography beamlines. *J. Synchrotron Radiat. 9* (Part 6), 401−406.
(35) McCoy, A. J., Grosse-Kunstleve, R. W., Adams, P. D., Winn, M. D., Storoni, L. C., and Read, R. J. (2007) Phaser crystallographic software. *J. Appl. Crystallogr. 40* (Part 4), 658−674.
(36) Adams, P. D., Afonine, P. V., Bunkoczi, G., Chen, V. B., Davis, I. W., Echols, N., Headd, J. J., Hung, L. W., Kapral, G. J., Grosse-Kunstleve, R. W., McCoy, A. J., Moriarty, N. W., Oeffner, R., Read, R. J., Richardson, D. C., Richardson, J. S., Terwilliger, T. C., and Zwart, P. H. (2010) PHENIX: A comprehensive Python-based system for macromolecular structure solution. *Acta Crystallogr. D66* (Part 2), 213−221.
(37) Emsley, P., Lohkamp, B., Scott, W. G., and Cowtan, K. (2010) Features and development of Coot. *Acta Crystallogr. D66* (Part 4), 486−501.
(38) Chen, V. B., Arendall, W. B., III, Headd, J. J., Keedy, D. A., Immormino, R. M., Kapral, G. J., Murray, L. W., Richardson, J. S., and Richardson, D. C. (2010) MolProbity: All-atom structure validation for macromolecular crystallography. *Acta Crystallogr. D66* (Part 1), 12−21.
(39) Davis, I. W., Leaver-Fay, A., Chen, V. B., Block, J. N., Kapral, G. J., Wang, X., Murray, L. W., Arendall, W. B., Snoeyink, J., Richardson, J. S., and Richardson, D. C. (2007) MolProbity: All-atom contacts and structure validation for proteins and nucleic acids. *Nucleic Acids Res. 35* (Web Server Issue), W375−W383.
(40) Kontopidis, G., Wu, S. Y., Zheleva, D. I., Taylor, P., McInnes, C., Lane, D. P., Fischer, P. M., and Walkinshaw, M. D. (2005) Structural and biochemical studies of human proliferating cell nuclear antigen complexes provide a rationale for cyclin association and inhibitor design. *Proc. Natl. Acad. Sci. U.S.A. 102* (6), 1871−1876.
(41) Dundas, J., Ouyang, Z., Tseng, J., Binkowski, A., Turpaz, Y., and Liang, J. (2006) CASTp: Computed atlas of surface topography of proteins with structural and topographical mapping of functionally annotated residues. *Nucleic Acids Res. 34* (Web ServerIssue), W116−W118.
(42) Fridman, Y., Gur, E., Fleishman, S. J., and Aharoni, A. (2013) Computational protein design suggests that human PCNA-partner interactions are not optimized for affinity. *Proteins 81* (2), 341−348.
(43) Kanagaraj, R., Saydam, N., Garcia, P. L., Zheng, L., and Janscak, P. (2006) Human RECQ5β helicase promotes strand exchange on synthetic DNA structures resembling a stalled replication fork. *Nucleic Acids Res. 34* (18), 5217−5231.
(44) Hamajima, N., Johmura, Y., Suzuki, S., Nakanishi, M., and Saitoh, S. (2013) Increased Protein Stability of CDKN1C Causes a Gain-of-Function Phenotype in Patients with IMAGe Syndrome. *PLoS One 8* (9), e75137.
(45) Cazzalini, O., Perucca, P., Mocchi, R., Sommatis, S., Prosperi, E., and Stivala, L. A. (2014) DDB2 association with PCNA is required for its degradation after UV-induced DNA damage. *Cell Cycle 13* (2), 240−248.
(46) Chen, X., Paudyal, S. C., Chin, R. I., and You, Z. (2013) PCNA promotes processive DNA end resection by Exo1. *Nucleic Acids Res. 41*, 9325−9338.
(47) Howlett, N. G., Harney, J. A., Rego, M. A., Kolling, F. W. t., and Glover, T. W. (2009) Functional interaction between the Fanconi Anemia D2 protein and proliferating cell nuclear antigen (PCNA) via a conserved putative PCNA interaction motif. *J. Biol. Chem. 284* (42), 28935−28942.
(48) Bacquin, A., Pouvelle, C., Siaud, N., Perderiset, M., Salome-Desnoulez, S., Tellier-Lebegue, C., Lopez, B., Charbonnier, J. B., and Kannouche, P. L. (2013) The helicase FBH1 is tightly regulated by PCNA via CRL4(Cdt2)-mediated proteolysis in human cells. *Nucleic Acids Res. 41* (13), 6501−6513.
(49) Parker, A., Gu, Y., Mahoney, W., Lee, S. H., Singh, K. K., and Lu, A. L. (2001) Human homolog of the MutY repair protein (hMYH) physically interacts with proteins involved in long patch DNA base excision repair. *J. Biol. Chem. 276* (8), 5547−5555.
(50) Banks, D., Wu, M., Higa, L. A., Gavrilova, N., Quan, J., Ye, T., Kobayashi, R., Sun, H., and Zhang, H. (2006) L2DTL/CDT2 and PCNA interact with p53 and regulate p53 polyubiquitination and protein stability through MDM2 and CUL4A/DDB1 complexes. *Cell Cycle 5* (15), 1719−1729.
(51) Shibata, E., Dar, A., and Dutta, A. (2014) CRL4Cdt2 E3 Ubiquitin Ligase and PCNA Cooperate to Degrade Thymine DNA Glycosylase in S-phase. *J. Biol. Chem. 289*, 23056−23064.
(52) Park, J. M., Yang, S. W., Yu, K. R., Ka, S. H., Lee, S. W., Seol, J. H., Jeon, Y. J., and Chung, C. H. (2014) Modification of PCNA by ISG15 plays a crucial role in termination of error-prone translesion DNA synthesis. *Mol. Cell 54* (4), 626−638.

DOI: 10.1021/acs.biochem.5b00241
Biochemistry 2015, 54, 3483−3493